Monthly Notices
of the
ROYAL ASTRONOMICAL SOCIETY

MNRAS **492,** 5141–5151 (2020)
Advance Access publication 2020 January 15

doi:10.1093/mnras/staa103

Activity and differential rotation of the early M dwarf Kepler-45 from transit mapping

S. M. Zaleski [1]★ A. Valio,[2] B. D. Carter[1] and S. C. Marsden[1]

[1]*Centre for Astrophysics, University of Southern Queensland, Toowoomba, QLD 4350, Australia*
[2]*Center for Radio Astronomy and Astrophysics, Mackenzie Presbyterian University, Rua da Consolaçao, 896, São Paulo, SP 01302-907, Brazil*

Accepted 2020 January 6. Received 2019 December 17; in original form 2019 October 31

ABSTRACT

Little is known of the activity and differential rotation of low luminosity, early M dwarfs from direct observation. We present the first stellar activity analysis of star-spots and faculae for the hot Jupiter hosting M1V dwarf Kepler-45 from *Kepler* transit light curves. We find star-spot and facula temperatures contrasting a few hundred degrees with the quiet photosphere, hence similar to other early M dwarfs having a convective envelope surrounding a radiative core. Star-spots are prominent close to the centre of the stellar disc, with faculae prominent towards the limbs, similar to what is observed for the Sun. Star-spot and facula mean sizes are about 40 and 45 $\times$ 10^3 km, respectively, and thus faculae occupy a 10 per cent larger surface area than the star-spots. A short-term activity cycle of about 295 d is observed that is reminiscent of those seen for other cool dwarfs. Adopting a solar-type differential rotation profile (faster equatorial rotation than polar rotation), our star-spot and facula temporal mapping indicates a rotation period of 15.520 $\pm$ 0.025 d at the transit latitude of -33.2°. From the mean stellar rotation of 15.762 d, we estimate a rotational shear of 0.031 $\pm$ 0.004 rad d^{-1}, or a relative differential rotation of 7.8 $\pm$ 0.9 per cent. Kepler-45's surface rotational shear is thus consistent with observations and theoretical modelling of other early M dwarfs that indicate a shear of less than 0.045 rad d^{-1} and no less than 0.03 rad d^{-1} for stars with similar stellar rotation periods.

Key words: stars: activity – stars: solar-type – starspots.

1 INTRODUCTION

M dwarfs are the most plentiful stars in the Galaxy. These cool, faint stars, having smaller radii and masses than the Sun, are found throughout the Solar neighbourhood, comprising 70 per cent of the stellar population (Bochanski et al. 2010). M dwarfs fill the lower end of the main sequence on the Hertzsprung–Russell (H–R) diagram with an effective temperature scale of roughly 4000 K for early M dwarfs to 2000 K for late (ultracool) M dwarfs (Rajpurohit et al. 2013). Their abundance and physical properties have made M dwarfs popular targets in the search for Earth-sized and Earth-like exoplanets in the habitable zone, where radiation heating and greenhouse effects favour the existence of liquid water on a planet's surface. Since M dwarfs are small low-mass stars, the ratios of exoplanet radius and mass to stellar radius and mass will be greater than for other cool stars targeted for planet searches. This will produce a more notable flux reduction in photometric time series as a planet blocks light from the star and a larger variation in Doppler measurements of stellar motion.

Radial velocity surveys were the first technique used for discovering planets around M dwarfs. In 1998, the first Jupiter mass planet was discovered orbiting the M dwarf GJ 876 (M4V) (Delfosse, Forveille & Mayor 1998; Marcy et al. 1998). Since then, radial velocity searches including M dwarf stars have been augmented by information from star-spots via targeted photometric follow-up. The presence of star-spots plays a discriminating role in the confirmation of candidate exoplanets orbiting M dwarfs, as well as other stars. The stellar rotation that brings star-spots in and out of view produces photometric variability useful to measure rotation period but will distort absorption line profiles and create radial velocity jitter (Saar & Donahue 1997; Barnes, Jeffers & Jones 2011). Nevertheless, a planet may be identified if its radial velocity signature is greater than spot induced jitter and a stellar rotation period measured from spot modulation can be used to separate the effects of activity from reflex motion due to a planet (Boisse et al. 2011; Diez Alonso et al. 2019).

The *Kepler* mission revolutionized the search for exoplanets by introducing the transit method as a new application of photometry (Borucki 2010). Though the main objective of the *Kepler* mission was to discover Earth-sized planets in the habitable zones of Sun-like stars via the loss of stellar flux due to planetary transits, the abundance of photometric data collected for a vast assortment of

★ E-mail: shelley.zaleski@usq.edu.au

stellar spectral types at different ages has provided for the broad analysis of stellar behaviour. Listed in the NASA Exoplanet Archive are 418 confirmed hot Jupiters from programs including the *Kepler* mission (Thompson et al. 2016). Of those gas giants, 375 transit their host stars. The majority of confirmed hot Jupiters orbit F, G, and K stars (Bakos et al. 2018). The dearth of hot Jupiters found in M dwarf star–planet systems is not surprising in view of a favoured formation of small planets around low-mass, cool stars (Apai & Pascucci 2010). Only five hot Jupiters are known to orbit M dwarfs. Kepler-45b (Johnson, Gazak & Apps 2012), HATS-6b (Hartman et al. 2015), NGTS-1b (Bayliss et al. 2018), and HATS-71b (Bakos et al. 2018) were discovered via transit surveys, whereas HD 41004B-b (Zucker et al. 2003) was discovered from radial velocity measurements.

Kepler-45b transits an M1V dwarf in a single planet system. The Kepler-45 system offers an uncommon opportunity to investigate the magnetic activity of an early M dwarf (a low-mass star hosting a hot Jupiter) through precise measurement of star-spot and facula physical parameters, which include radius, intensity, longitude, and latitude, for those features occulted during planetary transits. The transit depth resulting from the occultation of the stellar surface by a Jovian-sized planet provides the resolution necessary to distinguish the bumps and dips in transit light curves caused by star-spots and faculae, the features appearing in the photosphere that witness the action of an internal dynamo. Moreover, the area coverage of spots, at least within the transit band, can be associated with the observed total out-of-transit variability of the light curve (Basri et al. 2011).

Early M dwarfs, such as Kepler-45, have an internal Sun-like structure comprised of a large convective envelope surrounding a small radiative core. The magnetic activity in stars of this structure is thought to be induced by an $\alpha\Omega$ dynamo. The $\alpha\Omega$ dynamo based on our knowledge of the Sun is the accepted benchmark for magnetic activity in main-sequence F, G, and K solar-type stars (Fabbian et al. 2017). Magnetic fields are stretched by differential rotation (Ω-effect), twisted by the Coriolis force (α-effect), and pumped via magnetic buoyancy to the stellar surface. Magnetic fields appear as cool, dark star-spots and hot, bright faculae. The apparent motion of these emanating regions is driven by stellar rotation. The rotation periods of star-spots and faculae on the surface of solar-type stars vary with latitude. This differential rotation is a fundamental descriptor of the rotation profile of Sun-like stars (Charbonneau 2010). Rotational shear is greatest at the tachocline, the boundary between the radiative and convective zones. A transition from partially to fully convective stars occurs around spectral type M3V, where a notable gap in the H–R diagram marks the conversion from an $\alpha\Omega$ dynamo to an α^2 dynamo (Jao et al. 2018). A fully convective dynamo lacks a tachocline, a fundamental element of a solar-type dynamo model responsible for magnetic field generation. Late-type M dwarfs are also magnetically active (West et al. 2011), but star-spots on the surface of these fully convective stars may instead be due to a magnetic field generated by helical turbulence (Durney, De Young & Roxburgh 1993) or radiative diffusive heat flux (Fan & Fang 2014).

Does a standard for the behaviour of FGK solar-type stars based on stellar age or effective temperature extend to include early M dwarf spectral types? Hartman et al. (2011) propose that the correlation between period and photometric activity for FGK and early M dwarfs is consistent with rotation age–activity mass relations. As FGK stars age, their angular velocity decreases. This results in reduced shearing of magnetic field lines at the tachocline, lessening spot coverage, changes in spot stability, and decreasing differential rotation. M dwarfs also exhibit slowing rotation accompanied by a decline in magnetic activity as their ages increase. However, the trend for solar-type stars is not as pronounced in M dwarfs (Barnes et al. 2011; West et al. 2008, 2011). Slowly rotating early M dwarfs seem to follow the trend of solar-type stars, but their rotation age–activity relation has not yet been well established (Kiraga & Stępień 2011). Changes in stellar age and behaviour do not necessarily occur at the same rates among spectral types. An M dwarf of the same age as a G star will have a longer rotation period due to the faster rotational braking of low-mass stars (Guinan & Engle 2009).

Barnes et al. (2005) and Balona & Obedigamba (2016) also found that decreasing stellar effective temperature and mass yield decrease shear and differential rotation. Quenching of the diffusive strength of the dynamo may result in star-spots decaying slower on cool, early M stars than they do on hotter FGK stars with equivalent rotation periods (Giles, Collier Cameron & Haywood 2017). Star-spot lifetimes on early M dwarfs derived from observation have not yet been well documented, thus restricting their discussion relative to star-spot lifetimes on other solar-type stars. Giles et al. (2017) estimated star-spot lifetimes for approximately 2200 Kepler stars divided into two sample groups with stellar rotation periods of 10 and 20 d. Though the number of M dwarfs in the samples was limited, they projected star-spot lifetimes of roughly 50–275 d for the faster rotators and roughly 10–450 d for the slower rotators. A comparison may be made between the star-spot lifetime of 100–300 d for G-type stars estimated by Mehrabi, He & Khosroshahi (2017) and the observed star-spot lifetimes on the mid-type dwarf GJ 1243 (M4V) (Davenport, Hebb & Hawley 2015). From photometric analysis, Davenport et al. (2015) report a long-lived star-spot (on the order of years) and multiple appearances of a spot lasting 100–500 d. This may be indicative of slower star-spot decay for M dwarfs.

Due to the difficulty of observation, much remains to be learned about the morphology of star-spots and faculae on low luminosity, slowly rotating M dwarfs. Examination of star-spot and facula sizes, distributions, and temperatures on those stars will provide valuable information on the effect of stellar mass and effective temperature on the dynamo and a basis for comparison with the dynamic processes in solar-type stars. We propose that transit photometry mapping is an effective means of determining stellar rotation and differential rotation for early M dwarfs. The light curve of an exoplanet transiting an active stellar surface has small, in-transit variations due to the crossing of star-spots and faculae. The width, height, and time of these variations may be converted into the physical characteristics of star-spots and faculae, i.e. radius, intensity, and longitudinal position (Silva 2003). Via transit photometry mapping, the characteristics of individual star-spots and faculae cumulatively build magnetic activity maps of the stellar surface. This technique (see Section 3) has been used to evaluate stellar activity and rotation at transit latitudes for solar-type stars CoRoT-2 (G7V) (Silva-Valio et al. 2010; Silva-Valio & Lanza 2011), Kepler-17 (G2V) (Valio et al. 2017), Kepler-63 (G5V) (Estrela & Valio 2016), and Kepler-71 (G7V) (Zaleski et al. 2019).

We have analysed the photometry of the red dwarf Kepler-45 and present the first compilation of individual star-spot and facula physical parameters for an early M dwarf. The observations are described in Section 2, and the model is explained in Section 3. The results are shown in Section 4, beginning with the modelled characteristics of the spots and faculae in Section 4.1. Photosphere to star-spot and facula temperature contrasts and magnetic activity cycle are presented in Sections 4.2 and 4.4. Mean stellar rotation period and rotational velocity are discussed in Section 4.5. We further provide an estimate of stellar rotation period and differential rotation at the transit latitude from the mapping of star-spot and facula longitudes along the transit chord, which is typically non-

Table 1. Kepler-45 system parameters.

Parameter	Value	Ref
Star		
Spectral type	M1V	1
Kepler magnitude (K_p)	15.979	2
Mass ($M_\odot$)	0.59 ± 0.06	1
Radius ($R_\odot$)	0.624 ± 0.019	3
Effective Temp (K)	3820 ± 90	1
Rotation Period (d)	15.762 ± 0.016	4
Rotational Velocity (km s^{-1})	$2.009^{+0.019}_{-0.07}$	4
Age (Gyr)	0.5	1
Limb darkening coeff 1, c_2	$1.45^{+0.04}_{-0.03}$	4
Limb darkening coeff 2, c_3	$-1.349^{+0.013}_{-0.012}$	4
Limb darkening coeff 3, c_4	$0.776^{+0.009}_{-0.010}$	4
Planet		
Mass ($M_{\rm Jup}$)	0.505 ± 0.090	1
Radius ($R_{\rm Jup}$)	$1.133^{+0.012}_{-0.011}$	4
Radius ($R_{\rm star}$)	$0.1823^{+0.0020}_{-0.0018}$	4
Semimajor axis (au)	$0.0314^{+0.0009}_{-0.0008}$	4
Semimajor axis ($R_{\rm star}$)	$10.82^{+0.32}_{-0.28}$	4
Inclination angle (°)	$87.10^{+0.32}_{-0.20}$	4
Orbital period (d)	2.455239 ± 0.000004	1
Eccentricity	$0.11^{+0.10}_{-0.09}$	1

Note. 1: Johnson et al. (2012), 2: Brown et al. (2011), 3: Berger et al. (2018), 4: Fit by authors in this work

equatorial, in Section 4.6. A summary and discussion of our results relative to the solar standard is given in Section 5.

2 KEPLER-45

Kepler-45 is an M1 dwarf star introduced by Borucki (2011) as Kepler Object of Interest KOI-254 (Kepler ID# 5794240) and studied by Johnson et al. (2012). Kepler-45 is a dim, cool dwarf with Kepler-band magnitude = 15.979 and $T_{\rm eff}$ = 3820 K. Its mass and radius are approximately 60 per cent of those of the Sun. Johnson et al. (2012) estimated a stellar rotation period of 15.8 ± 0.2 d and age of 0.5 Gyr, derived using the rotation period and gyrochronology relations published by Barnes (2010). A full set of system parameters is given in Table 1.

Kepler-45 is transited by a single hot Jupiter, Kepler-45b, with mass 0.505 $M_{\rm J}$ and radius 1.133 $R_{\rm J}$, in a 2.455 d orbit (refer to Table 1). Kepler-45b orbits its host star at a distance of 0.03 au, making it an excellent target for future study of the atmosphere of a planet receiving energy emitted from a cool host star (Shields, Ballard & Johnson 2017). A planet the size of Kepler-45b crossing a star whose radius is 60 per cent of the Sun's results in a transit depth up to 150 times greater than that due to an Earth-sized planet transiting the same sized star. The mean transit depth of Kepler-45b smoothed light curves is 3.52 per cent of normalized flux, with a maximum depth of 3.99 per cent. This significant transit depth increases the probability of extracting star-spots and faculae from noise in the transit light curve since these magnetic features generally cause less than a 0.5 per cent variation in stellar flux.

Kepler-45b transit light curves are contained in the NASA Exoplanet Archive at MAST, which is a repository of raw and pre-conditioned light curve data spanning the almost 4 yr of the *Kepler* mission (Thompson et al. 2016). The available pre-conditioned data, or Pre-search Data Conditioning Simple Aperture Photometry (PDCSAP), has been cleansed of systematic noise due to *Kepler*

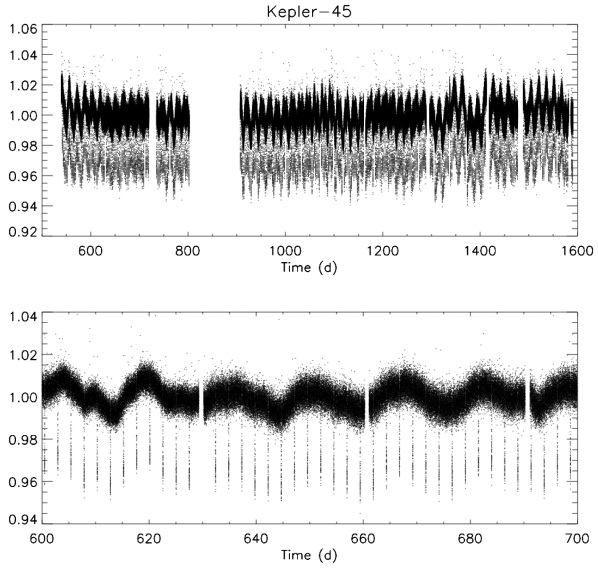

Figure 1. *Top:* Kepler-45 SC light curves for Quarters 6–8 and 10–17. Time in days corresponds to Barycentric Kepler Julian Date (BKJD). Observation began on 539.4608 BKJD and ended on 1591.0013 BKJD (2010 June 24–2013 May 11). *Bottom:* Enlargement of 100 early days of observation of Kepler-45.

telescope instrumentation (Jenkins et al. 2010; Smith et al. 2012; Stumpe et al. 2012). Data were recorded at the two sampling rates of the *Kepler* spacecraft, a long cadence (LC) mode of 29.4 min and a high temporal precision short cadence (SC) mode of 58.85 s. The PDCSAP SC data provide the temporal resolution required for the assessment of star-spots and faculae, whose presence lasts only minutes during a transit.

Johnson et al. (2012) used LC data from *Kepler* quarters 1 and 2, with supporting radial velocity measurements, adaptive optics imaging, and NIR spectroscopy to confirm the parameters of the Kepler-45 system. The unavailability of SC data for those early quarters precluded a detailed study of stellar magnetic activity. Thus, we augment the earlier work of Johnson et al. (2012) with our analysis of Kepler-45's photospheric activity and an estimate of stellar differential rotation at our computed transit latitude of −33.2°. Of interest to our investigation are the detrended PDCSAP SC light curves. Our analyses utilized the SC data in Kepler Data Release 25 (Thompson et al. 2016) available for 11 quarters: 6 through 8, beginning 2010 June 24 and ending 2011 March 24, and 10 through 17, beginning 2011 June 28 and ending 2013 May 11. The SC light curves for those quarters, as shown in Fig. 1, constitute observation for approximately 1000 d and contain 351 recorded transits out of 428 possible transits from the beginning of Quarter 6 to the end of Quarter 17. The depth of the transits and stellar rotation are evident.

2.1 Kepler-45b light curves

Kepler-45b probes the surface of its host star in a well-aligned, low obliquity orbit (Dai et al. 2018). The planet crosses its host star at stellar latitude $-33.2^\circ\ ^{+1.0}_{-0.9}$ (refer to Table 2 in the following section). The in-transit portion of each SC light curve is examined for potential star-spots and faculae, i.e. bumps and dips, along the transit chord. Figs 2 and 4 demonstrate the modulation in transit light curves due to the passage of the planet over star-spots and faculae. The normalized transit depth in both examples is 3.65 per cent, and

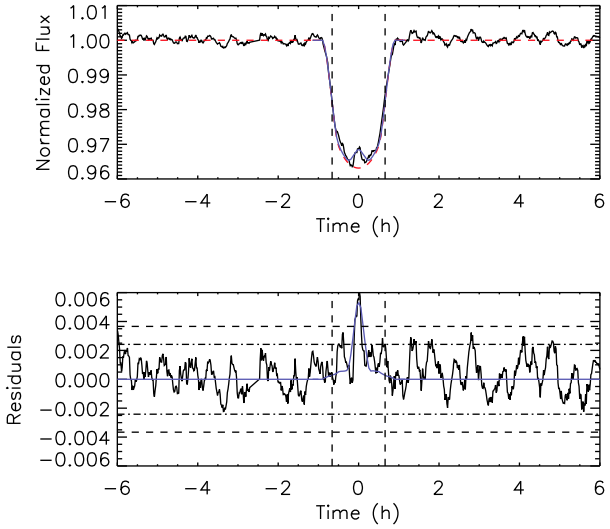

Figure 2. *Top:* SC light curve for Transit 97. The solid black line represents the observed data after 10 point smoothing. A potential star-spot is centred about $t = 0$, corresponding to 801.819 BKJD. The red dashed curve corresponds to the model of a spotless star, whereas the blue one is the result of the one spot fitting. The dashed vertical lines are $\pm 70^\circ$ from the centre of the stellar disc at $t = 0$. *Bottom:* Residuals resulting from the subtraction of the unspotted model from the smoothed transit data are shown by the solid black line. Star-spot residuals greatly exceed the rms noise, where the horizontal lines are ± 100 per cent (dashed) and ± 67 per cent (dash–dotted) of the unsmoothed out-of-transit rms noise, respectively. The blue line highlights the fit to the modelled spot.

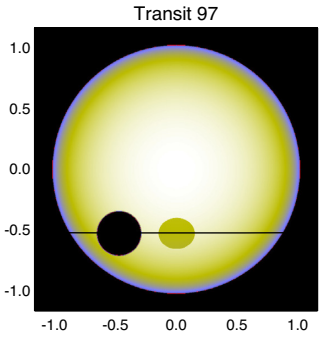

Figure 3. Image of the modelled star during Transit 97 with a single, big spot near the star's central meridian shown in grey. This spot is the result of the fit represented by the blue curves of Fig. 2. The planet is pictured as a black circle, with the horizontal line marking its transit path at -33.2°.

the transit duration is 1.820 ± 0.004 h. The example in Fig. 2 for Transit 97 shows a large star-spot centred at mid-transit ($t = 0$), pictured in Fig. 3. The time at mid-transit corresponds to 801.819 BKJD (Barycentric Kepler Julian Date defined as Barycentric Julian Day (BJD) minus an offset of 2454833 corresponding to 12:00 on 2009 January 1 UTC). In the upper panel of Figs 2 and 4, the irregular black curve represents observed data, which has been normalized and smoothed every 10 points. The smooth, U-shaped red dashed curve is the transit model for a spotless stellar surface as generated from system parameters. This model is detailed in Section 3. The blue curve is the result from one spot fitting, whose result is depicted in Fig. 3. The residuals resulting from the subtraction of the unspotted model from the smoothed data are shown in the lower panel in black and accentuate the star-spot's presence. The

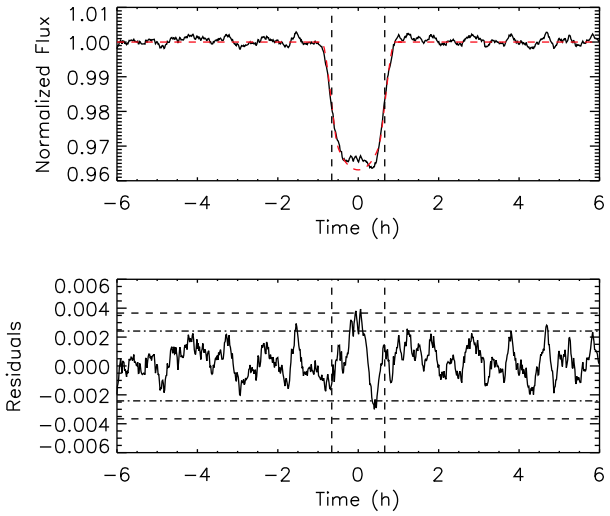

Figure 4. *Top:* SC light curve for Transit 5. The plotted quantities are the same as those defined for Fig. 2. The transit centre ($t = 0$) corresponds to 551.384 BKJD. *Bottom:* The residuals of potential star-spots near $t = 0$ exceed 100 per cent of the unsmoothed out-of-transit rms noise (dashed line). One potential facula near $t = 0.5$ h exceeds 67 per cent of the unsmoothed out-of-transit rms noise (dash–dotted line).

amplitude of its modulation is approximately 0.6 per cent. The model residual, depicted by the blue curve in the lower panel of Fig. 2, visualize our ability to replicate star-spot characteristics.

A spot group and a facula are evident in the Transit 5 light curve shown in Fig. 4. The star-spots appear near mid-transit, or 551.384 BKJD, with an amplitude of roughly 0.4 per cent, while the facula is apparent closer to the stellar limb with a dip of smaller amplitude of approximately 0.3 per cent.

3 THE MODEL

We have applied the model developed by Silva (2003), which simulates the passage of an exoplanet across a stellar disc. The stellar surface is defined as a 2D white light pixelated image. A three parameter limb darkening law is applied to the image (Sing et al. 2009) as given by

$$\frac{I(\mu)}{I(1)} = 1 - c_2(1-\mu) - c_3(1-\mu)^{3/2} - c_4(1-\mu)^2, \quad (1)$$

where $I(1)$ is the maximum intensity at disc centre, c_2, c_3, and c_4 are the limb darkening coefficients, and $\mu = \cos(\theta)$, where θ is the angle between the line of sight and the emergent intensity.

The planet is represented as a dark, opaque disc, with radius defined in units of stellar radius (depicted as the black circle in Fig. 3). Using the semimajor axis, period, and inclination angle of the planet's orbit (black horizontal line in Fig. 3), the planet's orbital position is calculated in 2 min increments from $t = -2$ h to $t = 2$ h, where $t = 0$ corresponds to mid-transit. At each time interval, the stellar intensity is calculated as the sum of all pixels in the stellar image. This produces a smooth transit light curve as a function of time (red dashed curves of Figs 2 and 4).

In light of the small eccentricity and low obliquity of the Kepler-45 system, we set two initial conditions for simulating the planet's orbit:

(i) The planet's orbit is circular (null eccentricity);
(ii) The planet's orbit is coplanar with the stellar equator (null obliquity).

Table 2. Secondary transit parameters of the Kepler-45 system.

Parameter	Value
Transit latitude (°)	$-33.2\ ^{+1.0}_{-0.9}$
Impact parameter	$0.548\ ^{+0.016}_{-0.014}$
Transit duration (h)	1.820 ± 0.004

With these conditions, the values for planet radius, semimajor axis, and inclination angle published by Johnson et al. (2012) were used to generate a preliminary model light curve. The model was then fit to an average of normalized and phase folded transits for all 11 *Kepler* quarters using an interactive data language (IDL) implementation of the Goodman & Weare (2010) Monte Carlo Markov Chain (MCMC) ensemble sampler to obtain the most probable parameter values and their uncertainties. The limb darkening coefficients were additionally fit in accordance with Kipping (2016)'s implementation of the three parameter limb darkening law (equation 1), which is based on analytic criteria for limiting combinations of coefficients to those that are physically plausible. The optimized parameters and coefficients are included in Table 1. Each value represents the median (50 per cent) of its sampling, with lower and upper 1σ errors corresponding to the 16 per cent and 84 per cent quantiles (Hogg & Foreman-Mackey 2018). We revised the values for planet radius, semimajor axis, and orbital inclination angle published by Johnson et al. (2012). The mean planet radius increased approximately 18 per cent from the value of 0.96 from Johnson et al. (2012) to 1.13 $R_{\rm Jup}$. The mean planet to stellar radius ratio increased 1.7 per cent from 0.179 to 0.182, and the scaled semimajor axis also increased 2.12 per cent from 10.6 to 10.82 stellar radii. The estimated mean stellar radius of 0.624 $R_\odot$ from Gaia Data Release 2 (DR2) was used for parameter scaling (Berger et al. 2018). The value from *Gaia* is approximately 13.5 per cent larger than the value of 0.55 $R_\odot$ first published by Johnson et al. (2012). The two values agree, however, within 1σ uncertainty. We also found that our estimate of $87.10^\circ\ ^{+0.32}_{-0.20}$ for orbital inclination angle agrees well with the value of $87.0^\circ \pm 0.7$ given by Johnson et al. (2012).

Impact parameter, transit latitude, and transit duration were computed from the fitted parameters and are given in Table 2. Impact parameter and transit latitude depend on inclination angle and semimajor axis as given by

$$b = \frac{a\cos(i)}{R_{\rm star}} \tag{2}$$

$$lat_{\rm tran} = \arcsin\left[\frac{a}{R_{\rm star}\cos(i)}\right], \tag{3}$$

where a is the semimajor axis, $R_{\rm star}$ is the stellar radius, and i is the inclination of the planet's orbit. The choice for transit projection to be in the Southern hemisphere is arbitrary (see Fig. 3). Transit duration is the difference between the times of ingress and egress in the model.

The smooth dashed red curves shown in the upper panels of Figs 2 and 4 represent the optimized model of a star without spots or faculae on its surface. The solid, irregular black curve represents the observed data after 10 point smoothing. When the model is subtracted from smoothed data, the residuals in the lower panels are obtained. The acceptance criteria which magnetic features must meet in order to be discerned from noise are represented by the horizontal lines in the lower panels, the double dot–dashed and dashed lines marking 67 per cent and 100 per cent of the out-of-transit rms, respectively. The rms noise for smoothed and unsmoothed data, both in and out-of-transit, is given in Table 3.

Table 3. RMS noise of Kepler-45 SC data.

Data	RMS
Unsmoothed	
In-transit	0.00379
Out-of-transit	0.00366
Smoothed	
In-transit	0.00145
Out-of-transit	0.00125

For both smoothed and unsmoothed data, the rms of the in-transit portion of all light curves is greater than the rms out-of-transit, inferring the existence of star-spots and faculae with amplitudes exceeding the noise. As may be noted from Figs 2 and 4, the out-of-transit residuals exceed rms values for smoothed data. Thus, we adopted the out-of-transit light-curve rms as a benchmark for evaluating potential star-spots and faculae in the residuals. Star-spot and facula residuals must either exceed ±100 per cent of the unsmoothed out-of-transit rms, or meet or pass ±67 per cent of the unsmoothed out-of-transit rms when transit noise is contained within ±67 per cent of the rms.

To determine the physical characteristics of magnetic features in a specific transit, those features are added to the surface of the modelled star to synthesize a spotted star transit model. A maximum of four features, either star-spots, faculae, or a combination of both, may be added as needed to fit an observed transit. While the number of features is variable, we found that a maximum of four features was enough to match the variations in observed transits. Star-spots and faculae are represented as dark and bright discs, respectively, and defined by radius, intensity, and longitude. Their latitude defaults to the transit projected latitude. The spotted model is fit to the observed transit light curve using an MCMC algorithm to determine probable values for these three physical characteristics for each spot. Intensity is defined relative to the stellar central intensity, $I(1) = 1$. Star-spot intensity must be less than $I(1)$ and greater than 0, and facula intensity must be greater than 1 but limited to 2. Mid-range values for intensity, $0.5\,I(1)$ for star-spots and $1.5\,I(1)$ for faculae, are inputs to the MCMC fit. Planet radius, $R_{\rm P}$, is defined in units of stellar radius, with an initial guess value of $0.5\ R_{\rm P}$. Longitude is defined with respect to 0° stellar topocentric longitude, which corresponds to the middle of the planet's projection on to the stellar disc at $t = 0$. Longitude is constrained to ±70° to avoid steep variations in intensity near the stellar limbs (Silva-Valio et al. 2010). The starting longitude for the fit is determined from the transit time at the centre of each star-spot or facula signature by

$$lon_{\rm sf} = \arcsin\left[\frac{a\cos\left(90^\circ - \frac{360^\circ\ t_{\rm sf}}{24\ P_{\rm orb}}\right)}{\cos(lat_{\rm tran})}\right], \tag{4}$$

where a is the semimajor axis, $P_{\rm orb}$ is the orbital period, $lat_{\rm tran}$ is the transit latitude, and $t_{\rm sf}$ is the time at star-spot or facula centre signature.

4 RESULTS

4.1 Star-spot and facula characteristics

The depth of Kepler-45b transits is variable, inferring photospheric activity. Does the M dwarf Kepler-45 indeed display the activity expected on cool stars with solar-type internal structure (Berdyugina 2004; Balona & Obedigamba 2016)? The presence of star-spots

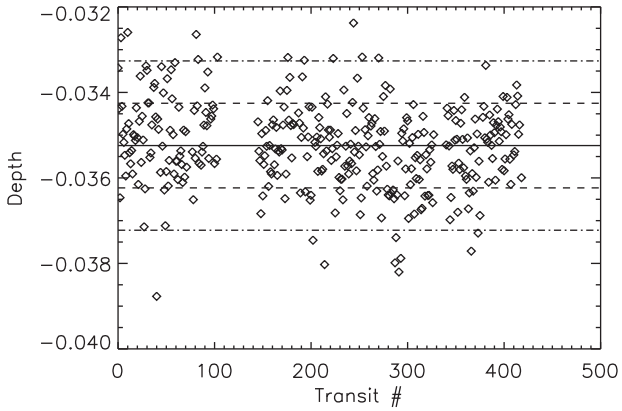

Figure 5. Change in transit depth as a function of transit number. All values are the difference relative to normalized flux (= 1). The solid line is the mean transit depth. The dashed and dash–dotted lines denote $\pm 1\sigma$ and $\pm 2\sigma$, respectively. Approximately 95 per cent of the transit depths are within $\pm 2\sigma$ of the mean.

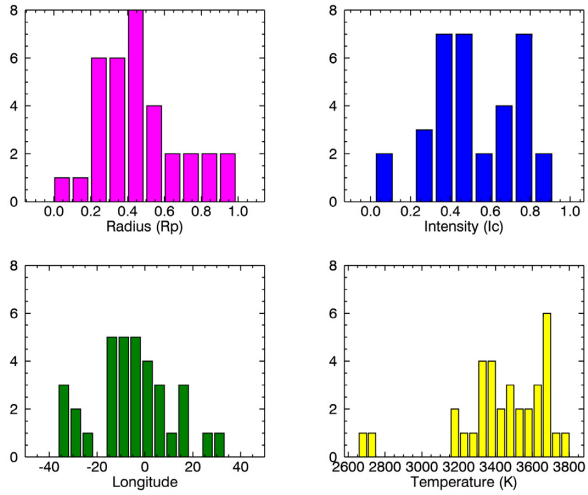

Figure 6. Histograms of star-spot parameters: radius and intensity (top row), and longitude in the observer's reference frame and temperature (bottom row).

will decrease the observed stellar flux, while faculae will add to the irradiance. Transit photometry mapping requires that the probing planet cross star-spots and/or faculae at the projected transit latitude. The depth variations observed for Kepler-45b at transit latitude -33.2° indicate such crossings.

The mean depth of Kepler-45b transits is 3.52 ± 0.10 per cent of normalized flux (= 1). Fig. 5 pictures the change in transit depth with transit number. A dispersion of estimated depths is anticipated since observed transit data have been smoothed every 10 points to preserve magnetic features and/or the irradiance of the observed stellar surface can vary with rotation. Close to 95 per cent of transit well depths fall within $\pm 2\sigma$ of the mean. The minimum and maximum transit depths are 3.238 per cent and 3.877 per cent, respectively. Transits are examined individually to determine (1) if the estimated depths are caused by noise or discontinuities, (2) if there are incomplete transits to eliminate, or (3) if magnetic signatures appear in complete and unbroken transits of any depth. Each continuous and complete transit is plotted against an unspotted model (red dashed curves of Figs 2 and 4) generated using the optimized orbital and

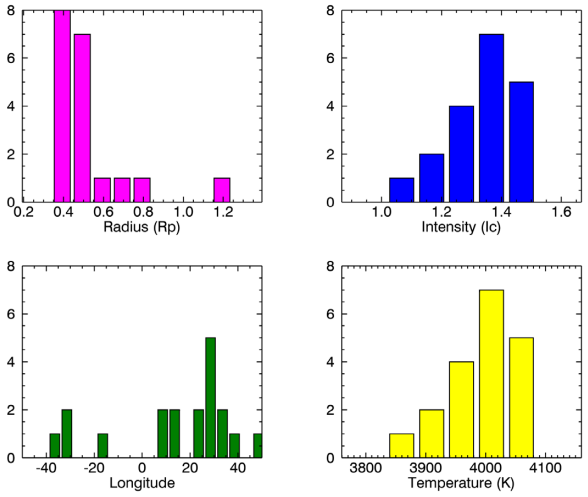

Figure 7. Histograms of facula parameters: radius and intensity (top row), and longitude in the observer's reference frame and temperature (bottom row).

stellar parameters. For those transits showing possible activity, the residuals resulting from the subtraction of the model from observed data are evaluated against the rms criteria given in Section 3. Star-spots and/or faculae in positively assessed transits are added to the spotless model and fit to the observed data on a per transit basis (see the preceding section, especially Figs 2, 3, and 4).

Star-spots and/or faculae were identified in 40 transits using the rms criteria and fit using MCMC. In total, 34 star-spots were found in 22 transits, and 19 faculae were detected in 18 transits. All but one facula appear as a single feature. Large star-spots suggesting spot groups were divided into multiple spots whenever possible. 14 of the star-spots fit were singletons, with the remaining star-spots divided among 6 pairs of spots, 2 sets of 3 spots, and 1 set of 2 spots with 1 facula.

Histograms of radius, intensity, and longitude are shown in Fig. 6 for star-spots and Fig. 7 for faculae. Star-spot mean radius is $0.51 \pm 0.22\ R_{\rm p}$, or equivalently $(40 \pm 17) \times 10^3$ km. The minimum and maximum star-spot radii are 0.04 and 0.98 $R_{\rm p}$, or 3×10^3 and 78×10^3 km. Faculae are approximately 10 per cent larger than the star-spots, with a mean radius of $0.57 \pm 0.20\ R_{\rm p}$, or $(45 \pm 16) \times 10^3$ km. The smallest facula has a radius of 0.39 $R_{\rm p}$, or 31×10^3 km, and the largest has a radius of 1.23 $R_{\rm p}$, or 98×10^3 km.

Mean star-spot intensity is 0.57 ± 0.22 I(1), and mean facula intensity is 1.37 ± 0.12 I(1), where $I(1)$ is the central intensity of the photosphere ($\mu = 1$). The intensities of star-spots are within the range of 0.07–0.96 $I(1)$. Facula intensities are within 1.07 and 1.49 $I(1)$. The intensity equivalent temperatures are discussed in Section 4.2.

Star-spot observation is generally greater in the central area of the stellar disc, while facula are perceived more commonly towards the stellar limbs. Star-spots are seen at longitudes spanning -34° to $+33^{\circ}$ along the transit chord in the reference frame of an observer on Earth, where 0° longitude is the central meridian of Kepler-45 at mid-transit. Faculae are discerned at longitudes -37° to $+49^{\circ}$. As may be noted in the longitude histograms, the majority of star-spots are observed within $\pm 20^{\circ}$ of the central meridian. Conversely, most faculae have longitudes $<-20^{\circ}$ or $>20^{\circ}$. This behaviour replicates that of their solar counterparts, where solar faculae are best observed close to the limb.

4.2 Star-spot and facula temperatures

Star-spot temperatures are one element in the understanding of convective flow suppression due to magnetic fields in active regions (Biazzo et al. 2006). From a compilation of star-spot contrasts, i.e. the temperature difference between star-spots and the photosphere, versus photosphere temperature for active stars, Berdyugina (2005) noted that contrast between star-spots and the photosphere decreases with decreasing stellar effective temperature. For example, star-spot contrast was approximately 500 K for a photosphere temperature of 3800 K and decreased to 200 K for a photosphere temperature of 3300 K. A later study of star-spot contrasts for dwarf stars by Mancini et al. (2017) contradicts this trend. They found no obvious dependence between contrast and effective temperature, or spectral class. Example dwarf stars of spectral types M2 and M4 had contrasts up to 850 K, comparable to the roughly 850 K contrast of the Sun, while hotter M dwarfs did not exceed contrasts of 600 K.

Much of what is known about star-spot physical properties on M dwarfs has come from TiO band spectroscopy (Fang et al. 2016). The transit method has provided a newer technique for determining physical properties. Of particular interest is the conversion of derived star-spot photometric intensity to temperature. Under the assumption that star-spots and the unspotted photosphere radiate as theoretical blackbodies, Planck's Radiation Law can be used to solve for star-spot temperature (Silva 2003). The ratio between star-spot and photosphere intensities is given by

$$\frac{I_{\rm spot}}{I_{\rm phot}} = \frac{\exp\left(\frac{hc}{\lambda K_{\rm B} T_{\rm eff}}\right) - 1}{\exp\left(\frac{hc}{\lambda K_{\rm B} T_{\rm spot}}\right) - 1}, \quad (5)$$

where h is Planck's constant, c is the speed of light, λ is the Kepler-band observation wavelength, $K_{\rm B}$ is Boltzmann's constant, and $T_{\rm eff}$ and $T_{\rm spot}$ are the photosphere and spot temperatures, respectively. The *Kepler* telescope's broad bandpass ranges from 420 to 900 nm, with optimal response at 600 nm.

Solving the above equation for $T_{\rm eff} = 3820$ K and $\lambda = 600$ nm yields a mean star-spot temperature of 3470 ± 250 K. As shown in the lower, right hand panel of Fig. 6, all but two star-spot temperatures lie within 3150–3800 K. The temperature contrast between the unspotted photosphere and the star-spots is $350\ ^{+260}_{-110}$ K. Berdyugina (2005) attributed low contrast in M dwarfs to either a larger contribution from the star-spot penumbra than from the umbra or small star-spot sizes. While we can estimate star-spot radii, the observed data do not permit delineation of umbral regions.

The mean temperature of the 19 modelled faculae calculated via equation (5) is 4020 ± 60 K, whereas the photospheric contrast is 200 ± 150 K. Solar faculae exhibit a similar contrast, differing from the quiet photosphere by a few hundred Kelvin (Solov'ev et al. 2019).

The star-spot to photosphere temperature ratio, $T_{\rm spot}/T_{\rm phot}$, falls in the range 0.68–0.97. These values are high compared to the ratio of 0.70 ± 0.05 for active G and K stars derived by O'Neal et al. (2004, 2006) from TiO band modelling. This may indeed infer a relatively moderate activity level for Kepler-45 as seen by the small number of star-spots at the transit latitude. From a study of all *Kepler* M dwarfs, Hawley et al. (2014) found that inactive early M dwarfs are less spotted than active mid M dwarfs.

4.3 Spot area coverage

While Kepler-45's photometric variability amplitude is significant, it cannot be used to predict the spot coverage of the entire stellar surface (Apai et al. 2018). The area covered by spots in time within the transit band of Kepler-45 is plotted in Fig. 8. Kepler-45 has a mean spotted area of 4.1 ± 2.5 per cent of the stellar surface (dashed horizontal line), which may contribute to the 3 per cent light-curve variability. The star-spots on Kepler-17, an active G2 star, are slightly larger than those on Kepler-45 (mean radius $(49 \pm 10) \times 10^3$ km) and cover an average area of 6 ± 4 per cent within the transit band 0° to -10° (Valio et al. 2017). Thus, the activity level of Kepler-45 is less than that of active G stars but greater than that of the current Sun.

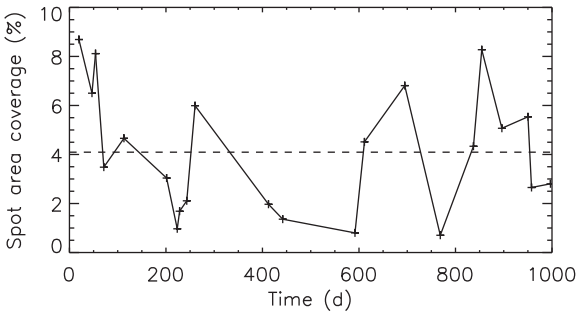

Figure 8. Area covered by spots within the occulted transit band of the surface of Kepler-45 for the whole observing period.

Doppler images of active early M dwarfs have shown that star-spots are distributed across the stellar surface, with no indication of dominant polar spots (Barnes et al. 2017 and references therein). In a Zeeman Doppler Imaging study of five slowly rotating, moderately active early M dwarfs (M0–M2), Hébrard et al. (2016) found that dark spots concentrate either close to the stellar magnetic pole or magnetic equator. Spots on the M0 dwarf GJ 410, whose physical properties of mass, radius, and rotation period are similar to those of Kepler-45, were found to concentrate towards the magnetic equator. The large-scale magnetic fields of GJ 410 and Kepler-45 may act similarly to the Sun's magnetic field, dictating the emergence of spots at solar latitudes.

4.4 Activity cycle

The strong magnetic fields of early M dwarfs may result in flaring rather than in organized spot emergence and cycles (Bondar 1995; Hathaway 2015). Yet, high-resolution spectra containing the Hα and/or Ca II K chromospheric indicators in conjunction with photometric data have been used to measure early M dwarf long-term activity cycles (Gomes da Silva et al. 2011; Astudillo-Defru et al. 2017; Küker et al. 2019). Long-term activity cycles are generally less than 8 yr (Küker et al. 2019). Bucconi et al. (2011) reported an activity cycle of approximately 4 yr for the M1 flare dwarf GI 229 A and approximately 7 yr for the M2.5 star GI 752 A. There remains no obvious correlation between rotation rate and cycle length (Savanov 2012; Küker et al. 2019).

Long-term activity cycles have been well studied for non-Kepler stars including M dwarfs (Oláh et al. 2009; Gomes da Silva et al. 2012; Savanov 2012; Robertson et al. 2013). Little appears in the literature concerning short-term cycles. While the observation span of the *Kepler* mission is insufficient for long-term cycle study, it does allow for examination of short-term cycles. Short-term cycles provide further evidence of the nature of the dynamo operating in early M dwarfs. Short-term cycles are known to exist in the Sun (Hathaway 2015). If early M dwarfs are truly solar-type stars, they should exhibit similar short-term cycles driven by an $\alpha\Omega$ dynamo.

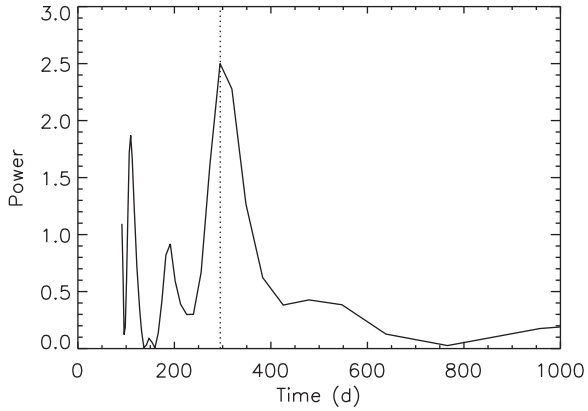

Figure 9. Activity cycle from Lomb–Scargle analysis of the total flux deficit due to star-spots per transit. The vertical dotted line intersects the curve at the peak power corresponding to a short activity cycle of 295 d.

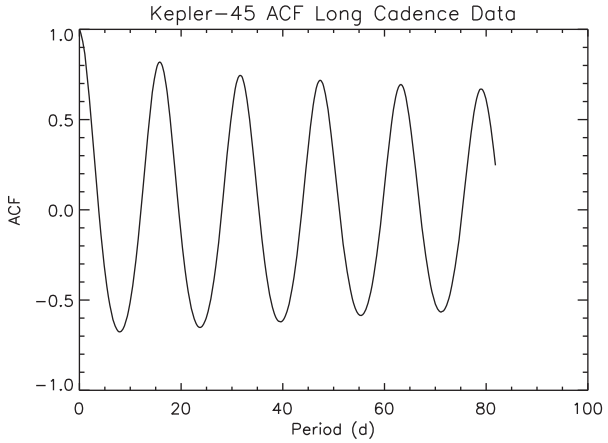

Figure 10. ACF of transit cleansed LC data for all quarters. The series of peaks corresponds to a mean stellar rotation period of 15.762 d.

Short-term cycles have been previously calculated from *Kepler* photometry (Vida, Oláh & Szabó 2014; Estrela & Valio 2016).

We see no evidence of flares in Kepler-45 light curves but do observe temporal recurrence of star-spots along the transit chord indicating possible cyclic behaviour. Short-term activity cycles may be derived from the temporal variation of the number of star-spots or the correlation of the total flux deficit per transit due to star-spots (Estrela & Valio 2017). Due to the sparsity of star-spots, we chose to employ the deficit method. Spot deficit is defined as effective spot area times surface intensity difference, or the central stellar intensity (= 1) minus spot intensity. The total flux deficit per transit is given by

$$F_{\rm def} = \sum r_{\rm spot}^2 (1 - I_{\rm spot}), \tag{6}$$

where $F_{\rm def}$ is the total flux deficit per transit due to spots, $r_{\rm spot}$ is spot radius, and $I_{\rm spot}$ is spot intensity.

Lomb–Scargle analysis of the total flux deficit per Kepler-45b transit yields a short magnetic activity cycle of 295 ± 50 d as shown by the dominant peak in Fig. 9. In comparison, the K4 dwarf HAT-P-11 (Kepler-3) has an activity cycle of 305 ± 60 d, derived from the flux deficit method (Estrela & Valio 2017), and the Sun has a short-term variability of roughly 154 d and quasi-biennial oscillation of 0.6–4 yr, deduced from daily sunspot numbers and sunspot areas (Zaqarashvili et al. 2010; Balogh et al. 2014; Hathaway 2015).

4.5 Mean stellar rotation period and rotational velocity

We verified the estimate of mean stellar rotation period for Kepler-45 published by Johnson et al. (2012), who used LC data from *Kepler* Quarters 1 and 2, and the later refined value of 15.816 ± 0.021 d published by McQuillan, Aigrain & Mazeh (2013), who used LC data from *Kepler* Quarters 1–4. The autocorrelation technique described in McQuillan, Mazeh & Aigrain (2014) was applied to all LC data for full Quarters 1 to 16 to recalculate the rotation period. The LC data were cleansed of transits and regridded to one continuous data set before performing the autocorrelation. The results are shown in Fig. 10. The slope of a line through the first four peaks yields a mean stellar rotation of 15.762 ± 0.016 d.

Using our estimate of mean stellar rotation period and the mean stellar radius of 0.624 $R_\odot$ from *Gaia* DR2, we calculate $v \sin i = 2^{+0.019}_{-0.070}$ km s^{-1}. Such low rotational velocities for early M dwarfs have been reported by Jeffers et al. (2018). They find that slow rotators of spectral type < M3.5V have $v \sin i < 5$ km s^{-1} and are Hα inactive.

4.6 Transit latitude rotation period and differential rotation

The model of a differentially rotating Sun, with rotation decreasing from the equator towards the poles, is the benchmark against which the latitudinal rotation of other stars is measured. If Kepler-45 rotates differentially, observed star-spots and faculae at latitudes less than 45° will move across the stellar face with a period less than the mean stellar rotation period. Thus, to evaluate the differential rotation of Kepler-45, first an estimate of the rotation at the transit latitude is needed. This was done using all the 53 features observed on the surface of Kepler-45.

Star-spot and facula longitudes are converted from the frame of an observer on Earth to the rotating frame of the star. The re-referenced longitudes are used to build a temporal map of the stellar surface at the mean stellar rotation period. The rotation period is then varied to find the one which best aligns the magnetic features with respect to longitude. The method is the same used previously for CoRoT-2 (Silva-Valio & Lanza 2011), Kepler-17 (Valio et al. 2017), and Kepler-71 (Zaleski et al. 2019).

The rotation period at the transit latitude of −33.2° that best aligns the magnetic features (star-spots and faculae) was found to be 15.520 ± 0.028 d. The reconstructed map of the stellar surface at that latitude, as a function of time, is shown in Fig. 11. Star-spot and facula concentrations are greatest at −110° and +10° as seen in the lower panel of Fig. 11. These concentrations may be indicative of active longitudes. The existence of active longitudes is anticipated on more active or rapidly rotating M dwarfs, paralleling the trend for young, solar-type stars (Lehtinen et al. 2016). Vida et al. (2010) located active regions separated by 120° on the M1-2 dwarf EY Dra ($v \sin i = 61$ km s^{-1}) (Jeffries, James & Bromage 1994).

Once the rotation period at the transit latitude has been determined, the differential rotation of the star can be estimated by assuming a differential rotation profile similar to the Sun's. In this case, we consider

$$\Omega(\alpha) = \Omega_{\rm eq} - \Delta\Omega \sin^2(\alpha), \tag{7}$$

where Ω is the angular velocity at a certain latitude, α, and $\Omega_{\rm eq}$ is the angular velocity at the stellar equator. $\Delta\Omega$ is the difference between the angular velocities at the equator and the pole, also known as rotational shear.

Assuming that the star-spots and faculae are present from the equator to the poles of the star, the resulting average rotation, $\bar{\Omega}$ is computed by integrating equation (7) from 0° to 90°. Thus the

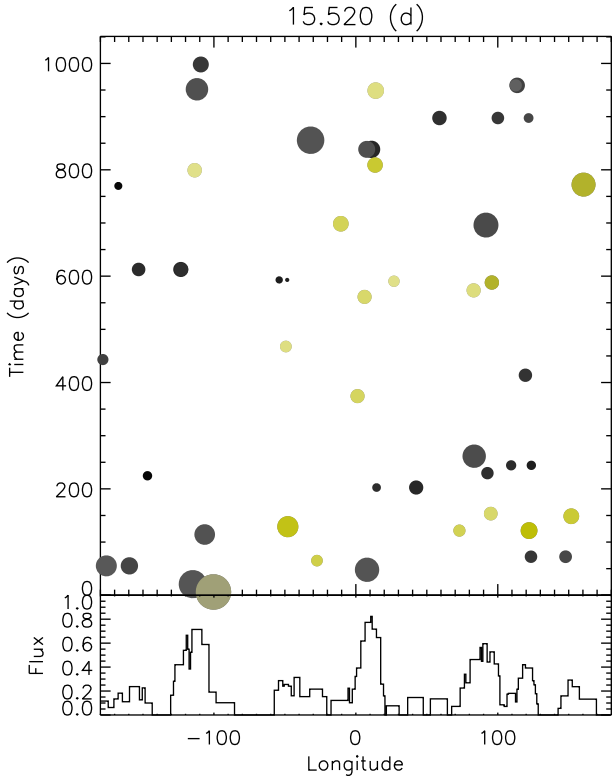

Figure 11. *Top:* Temporal map of the stellar surface at the transit latitude considering a period of 15.520 d. Star-spots are shown in shades of grey whereas faculae are shown in yellow. *Bottom:* The total flux difference from star-spots and faculae versus longitude.

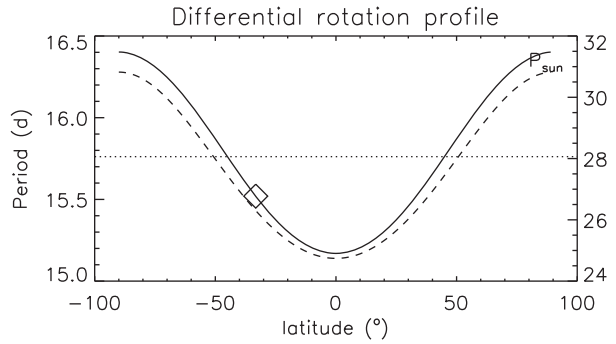

Figure 12. Differential rotation profiles of Kepler-45 (solid line) and the Sun (dashed line) as a function of latitude. The diamond marks the 15.520 d rotation period of Kepler-45 at transit latitude −33.2° estimated from transit mapping. The horizontal dotted line signifies the mean stellar rotation period of 15.762 d.

equation for the average angular rotation simplifies to

$$\bar{\Omega} = \Omega_{\rm eq} - \Delta\Omega/2. \quad (8)$$

The differential rotation profile of Kepler-45 is plotted in Fig. 12 as a function of latitude. The differential rotation profile of the Sun is included for comparison. The horizontal line indicates the 15.762 d mean stellar rotation period, and the diamond signifies the 15.520 d rotation period of Kepler-45 at the transit latitude.

Considering $\bar{\Omega} = 2\pi/P_{\rm rot}$, where $P_{\rm rot} = 15.762$ d is the average rotation period estimated in Section 2, we estimated $\Omega_{\rm eq} = 0.4142 \pm 0.0018 \pm$ rad d^{-1}, or $P_{\rm eq} = 15.17 \pm 0.07$ d, and $\Delta\Omega = 0.031 \pm 0.004$ rad d^{-1}, which yields a relative differential rotation of $\Delta\Omega/\bar{\Omega}$ of 7.8 ± 0.9 per cent. In a spectropolarimetric study of a small sample of M0–M3 dwarfs, Donati et al. (2008) detected rotational shears of 0.06–0.12 rad d^{-1}. They estimated that the M2.5 dwarf CE Boo, which is somewhat younger and smaller than Kepler-45 and has a rotation period of approximately 14 d, rotates differentially at a rate of no less than 0.03 rad d^{-1}. Reinhold, Reiners & Basri (2013) and later Reinhold & Gizon (2015) computed a relative shear between 0.01 and 0.11 rad d^{-1} for M dwarfs with $T_{\rm eff}$ between 3000 and 4000 K and a rotation period of approximately 15 d. Most recently, Küker et al. (2019) calculated that for early M dwarfs (0.66 $M_\odot$, $T_{\rm eff} = 4038$ K) shear increases from 0.028 to 0.047 rad d^{-1} as rotation period increases from 1 to 10 d and then decreases for longer periods due to reduction in the α dynamo effect. Their shear value for a rotation period of approximately 15 d is 0.045 rad d^{-1}.

5 SUMMARY AND DISCUSSION

This work presents the first robust analysis of stellar activity for a faint, early M dwarf from transit photometry. Kepler-45 is an M1V star with radius 0.624 $R_\odot$ and effective temperature of 3820 K. Given its low luminosity at Kepler magnitude 15.979 and moderately slow rotation period of 15.72 d, transit photometry becomes the best and only method for studying stellar activity. The hot Jupiter Kepler-45b is an optimal probe of its host star's surface as it passes between the star and the observer in a coplanar orbit. Kepler-45b (1.13 $R_{\rm Jup}$) orbits with a 2.45 d periodicity at a distance of 0.03 au. Photometric observation of Kepler-45 benefits from the radial size of Kepler-45b and its relatively short periodicity, yielding 351 deep transits in *Kepler* SC mode over the observation time of less than 4 yr. Only slightly more than 11 per cent of these recorded transits display discernible surface activity having flux variation greater than noise that may be attributed to star-spots and faculae.

We verified the mean rotation period through autocorrelation of transit-cleansed LC data (see Section 2). From our estimated rotation period and the mean stellar radius from *Gaia* DR2, we calculate a rotational velocity of 2 km s^{-1}. Early M dwarfs generally appear to have low rotational velocity (Kiraga & Stępień 2011). Reiners, Joshi & Goldman (2012) observed that early M dwarfs in a sample of spectral types M0–M4.5 rarely have a rotation velocity greater than 3 km s^{-1}. When considering a rotation–activity relation by which activity increases commensurate with increasing stellar rotation, we expect Kepler-45 to demonstrate relatively moderate activity as witnessed by the degree of spottedness (Messina et al. 2003; Kiraga & Stępień 2011). We found a modest amount of star-spots and faculae along transit latitude −33.2°, but unfortunately our method cannot project latitude dependent spottedness in light of the planet's orbital obliquity. Yet, the out-of-transit full-amplitude variability of approximately 3 per cent infers that star-spots appear at latitudes outside of the transit band. The source of Kepler-45's variability may be caused by small spots peppering the stellar surface beyond the transit band. Dark spots on early M dwarfs (M0–M2) were found to appear either close to the stellar magnetic pole or magnetic equator (Hébrard et al. 2016). They noted that spots on the M0 dwarf GJ 410, a star similar to Kepler-45, were concentrated towards the magnetic equator. This might imply that the spot area coverage for Kepler-45 is higher closer to the equator, assuming a solar-like spot distribution pattern. The spot area coverage is 4.1 ± 2.5 per cent at transit latitude −33.2°, thus at the upper limit in latitude where sunspots are detected.

The longitudes of star-spots and faculae detected on Kepler-45 follow the observational distribution of their solar counterparts. Sunspots are observed away from the solar limbs, while solar faculae are brighter and more visible towards the solar limbs. In the observer's reference frame, Kepler-45's star-spots are seen closer to the stellar disc centre than the faculae which are seen closer to the stellar limbs. Most star-spots have longitudes within $\pm 20^{\circ}$ of the centre of the stellar face (Fig. 6), while most faculae longitudes are $< -20^{\circ}$ or $> 20^{\circ}$ and as great as 49° (Fig. 7).

Spectroscopic analysis has largely been the knowledge source for star-spot temperature. The transit method is now stepping to the forefront. Morris et al. (2018) modelled star-spot sizes and temperatures for the M8V star TRAPPIST-1 using *Kepler* and *Spitzer* light curves. *Spitzer* data served to constrain star-spot radii and temperatures. Using only *Kepler* data, we simultaneously modelled star-spot and facula radii and intensities. Assuming that the magnetic features radiate as black bodies, we converted intensity to temperature for each feature. The mean star-spot temperature is 3470 ± 250 K. Relative to the stellar effective temperature of 3820 K, the mean contrast between star-spots and the unspotted photosphere is -350 K. Similarly, the mean facula temperature is 4020 ± 60 K, yielding a mean temperature contrast of $+200$ K. The contrasts are modest in relation to the solar contrast of -850 K and typical of the contrasts observed for other M dwarfs (Mancini et al. 2017).

Lomb–Scargle analysis of the irradiance loss due to star-spots yields a short-term activity cycle of 295 ± 50 d. Estrela & Valio (2016) estimated short activity cycles for two solar-type stars, 460 ± 60 d for Kepler-63 and 410 ± 50 d for Kepler-17. They also found a cycle of 305 ± 60 d for HAT-P-11 (Kepler-3), a spotted K4 dwarf (Estrela & Valio 2017). The short cycles may parallel short-term solar activity. A periodicity of roughly 154 d has been observed in solar cycles during times of maximum activity. This cycle may be indicative of the interaction of the local magnetic field and differential rotation (Zaqarashvili et al. 2010 and references therein). Quasi-biennial oscillations observed for the Sun occur on time-scales of 200 d to 4 yr. A possible explanation for these oscillations is the interplay of magnetic field components (Balogh et al. 2014). We propose that a dynamic dynamo drives Kepler-45's short-term periodicity as it does in the Sun.

As predicted by Donati et al. (2008) for early M dwarfs, we find rotation period to be latitude dependent. The 15.520 ± 0.025 d rotation period at the transit latitude calculated from correlation of flux difference due to star-spots and faculae at longitudes mapped in a frame rotating with the star is smaller than the 15.762 d mean period. Applying a solar differential profile, we estimate a rotational shear of $\Delta\Omega = 0.031 \pm 0.004$ rad d^{-1} and relative differential rotation of $\Delta\Omega/\bar{\Omega}$ of 7.8 ± 0.9 per cent. Over a decade ago, Reiners & Schmitt (2003) noted that slowly rotating solar-type stars had the most noticeable differential rotation. Their conclusion did not include M dwarfs. The trend was later confirmed by Reinhold et al. (2013) and Reinhold & Gizon (2015) for Kepler stars including M dwarfs. They calculated relative shear values between 0.01 and 0.11 rad d^{-1} for cool stars with a rotation period of roughly 15 d. Küker et al. (2019) later proposed a relative shear value of 0.045 rad d^{-1} for early M dwarfs (0.66 $M_{\odot}$, $T_{\rm eff} = 4038$ K) with the same rotation period. Our value lies within the range published by Reinhold & Gizon (2015) and is in line with the relative shear offered by Küker et al. (2019) given that Kepler-45 is somewhat cooler and less massive (0.59 $M_{\odot}$, $T_{\rm eff} = 3820$ K).

To summarize, this work has provided the first analysis of *Kepler* transit light-curve data for the hot Jupiter hosting early M dwarf Kepler-45, including mapping of star-spot and facula features. The results are consistent with observed solar-type spot activity, differential rotation, and sometimes rapid activity cycles observed for other red dwarfs, and demonstrate the ability of transit mapping to detail surface activity even for relatively faint red dwarf targets. The Kepler-45 system also provides a particular opportunity for future study of the impacts of host star activity on a close-in giant planet.

ACKNOWLEDGEMENTS

The authors would like to thank the anonymous referee for comments and suggestions that improved the content herein.

AV acknowledges partial financial support from Brazilian agency FAPESP (São Paulo Research Foundation) (# 2013/10559-5).

This paper includes data from the *Kepler* mission. Funding for the *Kepler* mission is provided by the National Aeronautics and Space Administration (NASA) Science Mission directorate. *Kepler* light-curve data were obtained from the NASA Exoplanet Archive, which provides public access to *Kepler* Mission data. The primary archive of all *Kepler* data is provided by the Mikulski Archive for Space Telescopes at the Space Telescope Science Institute (MAST at STScI). The Kepler Time Series Program Interface provides access to Kepler parameters. We thank the *Kepler* team for their efforts in providing the data and interfaces used in preparing this paper.

REFERENCES

Apai D., Pascucci I., 2010, Astrobiology Science Conference 2010, Evolution and Life: Surviving Catastrophes and Extremes on Earth and Beyond, League City, Texas
Apai D. et al., 2018, preprint (arXiv:1803.08708)
Astudillo-Defru N., Delfosse X., Bonfils X., Forveille T., Lovis, C, Rameau J., 2017, A&A, 600, A13
Bakos G. et al., 2018, preprint (arXiv:1812.09406v1)
Balogh A., Hudson H. S., Petrovay K., von Steiger R., 2014, Space Sci. Rev., 186, 1
Balona L. A., Obedigamba O. P., 2016, MNRAS, 461, 497
Barnes S. A., 2010, ApJ, 722, 2222
Barnes J. R., Collier Cameron A., Donati J. -F., James D. J., Marsden S. C., Petit P., 2005, MNRAS, 357, L1
Barnes J. R., Jeffers S. V., Jones H. R. A., 2011, MNRAS, 412, 1599
Barnes J. R., Jeffers S. V., Haswell C. A., Jones H. R. A., Shulyak D., Pavlenko Ya. V., Jenkins J. A., 2017, MNRAS, 471, 811
Basri G. et al., 2011, ApJ, 141, 20
Baylis D. et al., 2018, MNRAS, 475, 4467
Berdyugina S. V., 2004, Sol. Phys., 224, 123
Berdyugina S. V., 2005, Living Rev. Sol. Phys., 2, 8
Berger T. A., Huber D., Gaidos E., van Saders J. L., 2018, ApJ, 866, 99
Biazzo K., Frasca A., Catalano S., Marilli E., Henry G. W., Taz G., 2002, Mem. Soc. Astron. Ital. Suppl., 2, 220
Bochanski L. L., Hawley S. L., Covey K. R., West A. A., Ried I. N., Golimowski D. A., Ivezic Z., 2010, AJ, 139, 2679
Boisse I., Bouchy F., Hébrard G., Bonfils X., Santos N., Vauclair S., 2011, Proc. IAU Symp. 273, The Physics of Sun and Star Spots. Kluwer, Dordrecht, p. 281
Bondar N. I., 1995, A&AS, 111, 259
Borucki W. J., 2010, Science, 327, 977
Borucki W. J. et al., 2011, ApJ, 728, 117
Brown T. M., Latham D. W., Everett M. E., Esquerdo G. A., 2011, AJ, 142, 112
Bucconi A. P., Diaz R. F., Luoni M. L., Abrevaya X. C., Mauas P. J. D., 2011, AJ, 141, 34
Charbonneau P., 2010, Living Rev. Sol. Phys., 7, 3

Dai F., Winn J. N., Berta-Thompson Z., Sanchis-Ojeda R., Albrecht S., 2018, AJ, 155, 177
Davenport J. R. A., Hebb L., Hawley S. L., 2015, ApJ, 806, 212
Delfosse X., Forveille T. S., Mayor M., 1998, A&A, 338, L67
Diez Alonso E. et al., 2015, ApJ, 621, A126
Donati J.-F. et al., 2008, MNRAS, 390, 545
Durney B. R., De Young D. S., Roxburgh I. S., 1993, Sol. Phys., 145, 207
Estrela R., Valio A., 2016, ApJ, 831, 57
Estrela R., Valio A., 2017, Proc. IAU Symp. 328, Living Around Active Stars. Kluwer, Dordrecht, p. 152
Fabbian D. et al., 2017, Astron. Nachr., 338, 753
Fan Y., Fang F., 2014, ApJ, 789, 1
Fang X.-S., Zhao G., Zhao J.-K., Chen Y.-Q., Kumar Y. B., 2016, MNRAS, 463, 2494
Giles H. A. C., Collier Cameron A., Haywood R. D., 2017, MNRAS, 472, 1618
Gomes da Silva J., Santos N. C., Bonfils X., Delfosse X., Forveille T., Udry S., 2011, A&A, 534, A30
Gomes da Silva J., Santos N. C., Bonfils X., Delfosse X., Forveille T., Udry S., Dumusque X., Lovis C., 2012, A&A, 541, A9
Goodman J., Weare J., 2010, Commun. Appl. Math. Comput. Sci., 5, 68
Guinan E. F., Engle S. G., 2009, Proc. IAU Symp. 258, The Ages of Stars. Kluwer, Dordrecht, p. 395
Hartman J. D. et al., 2011, ApJ, 141, 5
Hartman J. D. et al., 2015, AJ, 149, 166
Hathaway D. H., 2015, Living Rev. Sol. Phys., 12, 2
Hawley S. L., Davenport J. R. A., Kowalski A. F., Wisniewski J. P., Hebb L., Dietrick R., Hilton E. J., 2002, ApJ, 797, 121
Hébrard É. M., Donati J.-F., Delfosse X., Morin J., Moutou C., Boisse I., 2016, MNRAS, 461, 1465
Hogg D. W., Foreman-Mackey D., 2018, ApJS, 236, 11
Jao W.-C., Henry T. J., Gies D. R., Hambly N. C., 2018, ApJ, 861, L11
Jeffers S. V. et al., 2018, A&A, 614, A76
Jeffries S. D., James D. J., Bromage G. E., 1994, MNRAS, 271, 476
Jenkins J. M. et al., 2010, ApJ, 173, L87
Johnson J. A. et al., 2012, AJ, 143, 111
Kipping D. M., 2016, MNRAS, 455, 1680
Kiraga M., Stępień K., 2013, Acta Astron., 57, 149
Küker M., Rudiger G., Oláh K., Strassmeier K.-G., 2019, A&A, 622, A40
Lehtinen J., Jetsu L., Hackman T., Kajathari P., Henry G. W., 2016, A&A, 588, A38
Mancini L. et al., 2017, MNRAS, 465, 843
Marcy G. W., Butler R. P., Vogt S. S., Fischer D., Lissauer J. J., 1998, ApJ, 505, L147
McQuillan A., Aigrain S., Mazeh T., 2013, MNRAS, 432, 1203
McQuillan A., Mazeh T., Aigrain S., 2014, ApJS, 211, 24
Mehrabi A., He H., Khosroshahi H., 2017, ApJ, 834, 207
Messina S., Pizzolato N., Guinan E. F., Rodono M., 2003, A&A, 410, 671
Morris B. M., Agol E., Davenport J. R. A., Hawley S. L., 2018, ApJ, 857, 39
O'Neal D., 2006, ApJ, 645, 659
O'Neal D., Neff J. E., Saar S. H., Cuntz M., 2004, AJ, 128, 1802
Oláh K. et al., 2014, A&A, 501, 703
Rajpurohit A. S., Reylé C., Allard F., Homeier D., Schultheis M., Bessell M. S., Robin A. C., 2013, A&A, 556, A15
Reiners A., Schmitt J. H. M. M., 2003, A&A, 398, 647
Reiners A., Joshi N., Goldman B., 2012, AJ, 143, 93
Reinhold T., Gizon L., 2015, A&A, 583, A65
Reinhold T., Reiners A., Basri G., 2013, A&A, 560, A4
Robertson P., Endl M., Cochran W. D., Dodson-Robinson S. E., 2013, ApJ, 764, 3
Saar S. H., Donahue R. A., 1997, ApJ, 485, 319
Savanov I. S., 2012, Astron. Rep., 56, 716
Shields A. L., Ballard S., Johnson J. A., 2017, Phys. Rep., 663, 1
Silva A. V. R., 2003, ApJ, 585, L147
Silva-Valio A., Lanza A. F., 2011, A&A, 529, 36
Silva-Valio A., Lanza A. F., Alonso R., Barge P., 2010, A&A, 510, 25
Sing D. K., Désert J.-M., Lecavelier Des Etangs A., Ballester G. E., Vidal-Madjar A., Parmentier V., Hebrard G., Henry G. W., 2009, A&A, 505, 891
Smith J. C. et al., 2012, PASP, 124, 919
Solov'ev A. A., Kirichek E. A., 2019, MNRAS, 482, 5290
Stumpe M. C. et al., 2012, PASP, 124, 984
Thompson S. E. et al., 2016, Kepler Data Release Notes (KSCI-19065-002)
Valio A., Estrela R., Netto Y., Bravo J. P., de Medeiros J. R., 2017, ApJ, 835, 2
Vida K. et al., 2010, Astron. Nachr., 331, 250
Vida K., Oláh K., Szabó R., 2014, MNRAS, 441, 2744
West A. A., Hawley S. L., Bochanski J. J., Covey K. R., Reid I. N., Dhital S., Hilton E. J., Masuda M., 2008, AJ, 135, 785
West A. A. et al., 2011, AJ, 141, 97
Zaleski S. M., Valio A., Marsden S. C., Carter B. D., 2019, MNRAS, 484, 618
Zaqarashvili T. V., Carbonell M., Oliver R., Ballester J. L., 2010, ApJ, 709, 749
Zucker S., Mazeh T., Santos N. C., Udry S., Mayor M., 2003, A&A, 404, 775

This paper has been typeset from a TEX/LATEX file prepared by the author.